

Article

Acoustic Experimental Technology for Aircraft Nacelle Liner

Qun Yan ^{1,2,3,*}, Dongwen Xue ^{1,2,3}, Qinjin Mu ^{1,2,3}, Jiafeng Yang ^{1,2}, Xiang Gao ^{1,2} and Wenchao Huang ^{1,2}

¹ Key Laboratory of Aeroacoustics and Dynamics, Aircraft Strength Research Institute, Xi'an 710065, China

² Aviation Technology Key Laboratory of Aviation Acoustic and Vibration, Xi'an 710065, China

³ Shaanxi Key Laboratory of Shock, Vibration and Noise, Xi'an 710065, China

* Correspondence: qunyan_ac@163.com

Abstract: An aircraft nacelle acoustic liner is a key mean of aircraft noise reduction. The success of its design depends strongly on the development of experimental technology, which is generally divided into two stages: impedance eduction and the modal verification of acoustic performance. The comparative study summarizes the impedance eduction technology based on the in-situ method and the straight forward method, and the acoustic modal measurement and control technology, as well as their applications in the design of the acoustic liner of an engine intake and exhaust ducts. The results show that the in-situ method has higher accuracy at low frequencies, and the accuracies of both methods are decreased in the high frequency range. Both methods show an acceptable accuracy and good applicability in the mid-frequency range. A modal generator was designed and used to emit separate and pure acoustic modes in sequence, and a comparative test was carried out on the two types of acoustic liner. Compared with the seamed acoustic liner, the seamless acoustic liner significantly improved its noise reduction effect at the multi-acoustic modes and target frequencies, which further increases the overall reduction up to 5.2 dB. Through research, reliable and validated technologies of acoustic performance tests for a nacelle acoustic liner were established.

Keywords: nacelle; liner; noise control; acoustic impedance; acoustic modes; impedance eduction



Citation: Yan, Q.; Xue, D.; Mu, Q.; Yang, J.; Gao, X.; Huang, W. Acoustic Experimental Technology for Aircraft Nacelle Liner. *Aerospace* **2023**, *10*, 56. <https://doi.org/10.3390/aerospace10010056>

Academic Editor: Hua-Dong Yao

Received: 26 November 2022

Revised: 29 December 2022

Accepted: 30 December 2022

Published: 5 January 2023



Copyright: © 2023 by the authors. Licensee MDPI, Basel, Switzerland. This article is an open access article distributed under the terms and conditions of the Creative Commons Attribution (CC BY) license (<https://creativecommons.org/licenses/by/4.0/>).

1. Introduction

In recent decades, aircraft noise level has been greatly reduced. However, airlines and aircraft manufacturers are still required by airworthiness policies, green aviation goals and government agencies to further reduce aircraft noise level [1]. For contemporary passenger aircraft, the main noise source of the aircraft is its engine. During takeoff and cruise stages, the fan noise radiates outward through the inlet and the exhaust duct, which is the main component of engine noise [2,3]. After years of development, the use of an acoustic liner deployed on the nacelle inner boundary for noise reduction has become one main countermeasure to control engine fan noise. The successful design of a nacelle acoustic liner depends heavily on special acoustic performance verification experiments. The acoustic design of the nacelle acoustic liner is generally divided into two stages, each focusing on different purposes and verification objects. At the preliminary design stage, the designed acoustic impedance is verified by using acoustic impedance eduction technology. At the detailed design stage, scaled and full-size nacelle samples are tested to verify the overall acoustic effect with the aid of acoustic mode syntheses control and detection technology.

Impedance eduction experiment technology was developed to accumulate data for establishing an accurate acoustic impedance model or verify the impedance characteristics of the designed acoustic lining experimental piece. It is mainly used to measure the flat or curved shaped acoustic liner plate sample. In the early days, the Netherlands Aerospace Academy proposed and developed the in-situ method based on the definition of acoustic impedance, which has been widely used [4,5]. One of its shortcoming is it can only be applied to the acoustic liner of a traditional sandwich structure. NASA proposed an inverse method [6–9] based on the idea of the impedance boundary assumption and

matching in a flow tube, which is applicable to more types of acoustic liners, but the data processing is time consuming. Jing Xiaodong et al. proposed the direct impedance extraction method [10] and transverse wave number method [11] based on the Prony method, and found that the experimental efficiency is highly improved compared with the inverse method. However, for the application scope of different impedance eduction techniques, as well as the requirements for frequency range and modal characteristics in the experiment, research activities are still undertaken.

On the other hand, experiments using scaled and full-size barrel or annular-shaped nacelle samples to verify the overall acoustic performance mainly concern the modal suppression/scattering characteristics, evaluating sound propagation prediction tools, and verifying the effect of the optimal design of acoustic liner spatial layout as main tasks for carrying out such experiments. In the research of NASA's program [12,13], and another projects conducted by DLR [14], a full scale or reduced scale fan is used as the acoustic source. An acoustic mode detection device is used to study the acoustic mode scattering and reduction as fan noise passing through the acoustic liner. The far-field directivity measurement is often used to measure the far-field directivity manipulation and study the noise reduction characteristics of the acoustic liner. The disadvantage of such experiments is that the order of the acoustic mode generated by the fan as the noise source is fixed, which cannot be adjusted and accurately controlled according to extended experimental needs, results in insufficient verification of the noise reduction performance of the acoustic liner.

In a current study, China Aircraft Strength Research Institute (ASRI) has further developed acoustic impedance eduction technology, where the application range of different impedance eduction methods is analyzed and compared. The noise reduction character of scaled and full-size nacelle liners was tested using one newly developed acoustic spinning mode syntheses generator to simulate the fan sound source, which realized the accurate control of the single acoustic mode or modes combination for detailed test use. A workflow of the current research in this paper is shown in Figure 1.

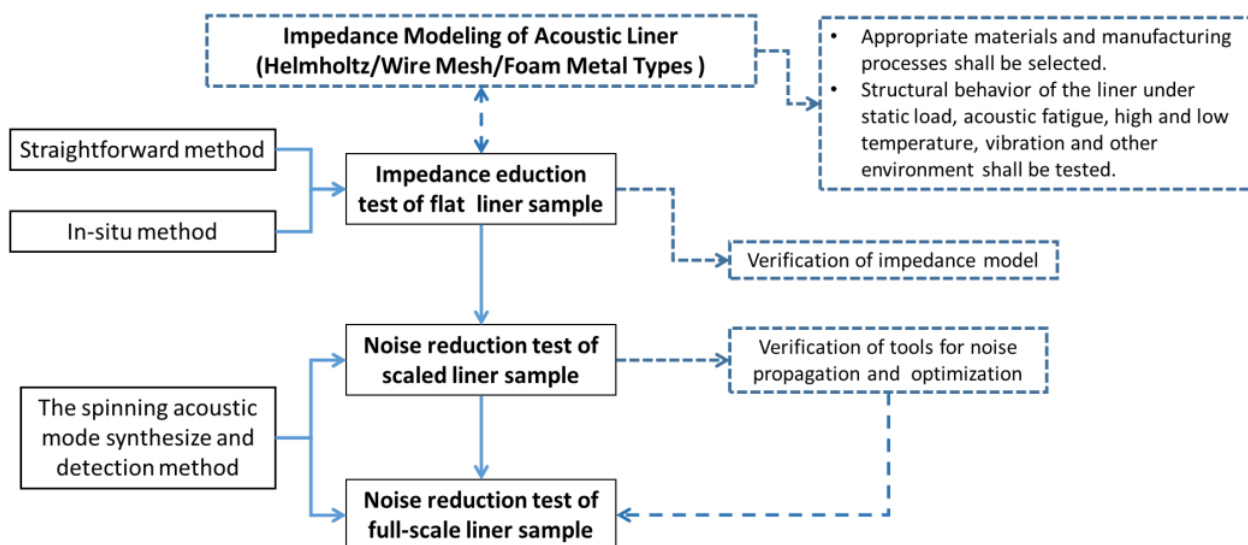


Figure 1. A workflow of activities and outcome in current research.

The impedance model of the wire mesh acoustic liner has been preliminarily established in the early stage. In this paper, the straightforward method and the in-situ method are used to educe impedance and the developed impedance model is verified. Most importantly, the application frequency range and accuracy of the two impedance extraction methods are analyzed. Some extra tasks not detailed nor included in this paper are those concerning static load, acoustic fatigue, high and low temperature, vibration and other strength tests of the liner that are carried out simultaneously. Furthermore, appropriate materials and manufacturing processes are selected. Secondly, the noise reduction test is

carried out for the scaled acoustic liner. In this experiment, the acoustic mode generator technology is used to simulate and control the frequency and amplitude of the dominant acoustic mode in the duct. Finally, the noise reduction test is carried out for the full-size acoustic liner test piece.

2. Acoustic Impedance Eduction Technology

2.1. Impedance Eduction Methodology

Dean from the Netherlands Aerospace Academy (NLR) proposed a technique for measuring the acoustic impedance with two microphones [4]. Figure 2 shows a typical resonance unit of a single degree of freedom Helmholtz resonant type of liner.

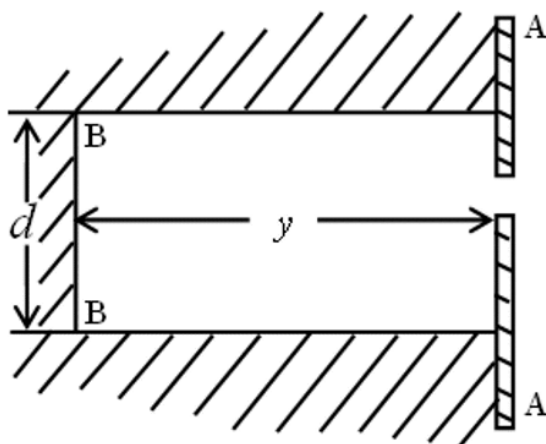


Figure 2. Typical resonance unit of a single degree of freedom Helmholtz resonant type of liner.

The incident sound wave can be expressed as

$$\bar{p}_i = p_0 e^{j(\omega t + k_i y)} \quad (1)$$

where: \bar{p}_i is the sound pressure obtained after taking the real part, which changes according to the sine law; p_i is the complex amplitude of sound pressure; ω is frequency; k_i is the incident wave number; and y is the position in the direction of acoustic liner thickness.

The sound wave reflected by the backplane can be expressed as

$$\bar{p}_r = p_0 e^{j(\omega t - k_r y)} \quad (2)$$

where the incident acoustic wave number k_i is equal to the reflected acoustic wave number k_r , which makes $k_i = k_r = k$, and $k = \omega/c$.

The velocity at section A-A is

$$u_A = -\frac{p_0}{\rho c k} e^{j\omega t} \left(k_i e^{jk_i y_A} - k_r e^{-jk_r y_A} \right) \quad (3)$$

where ρ is the local air density and y_A is the cavity depth. From the definition of acoustic impedance

$$z = \frac{\bar{p}_A}{u_A} = -\frac{\bar{p}_A}{\bar{p}_B} \rho c \frac{2k}{k_i e^{jk_i y_A} - k_r e^{-jk_r y_A}} \quad (4)$$

Set $\bar{p}_A = p_A e^{j(\omega t + \Phi_A)}$ and $\bar{p}_B = p_B e^{j(\omega t + \Phi_B)}$, so the acoustic impedance at section A-A is

$$z = -10^{\left(\frac{SPL_A - SPL_B}{20}\right)} \frac{(\sin \Phi - j \cos \Phi)}{\sin(ky_A)} \quad (5)$$

where $\Phi = \Phi_A - \Phi_B$ is the phase difference between sections A-A and B-B; and SPL_A and SPL_B are sound pressure levels of p_A and p_B , respectively.

If the sound pressure level difference and phase difference at A-A and B-B sections in Figure 1 are measured, the acoustic impedance of the single degree of freedom Helmholtz resonance type acoustic liner can be obtained. During the specific implementation, one can use dual channel equipment to measure the signal amplitude at A-A and B-B sections, and measure the phase difference through cross spectral analysis. Hence, the acoustic impedance can be calculated. In practice, the in-situ method requires insertion of the microphone into the acoustic liner, which will damage the physical structure of the acoustic liner. At the same time, the position of the sensor is required to be very accurate, and special installation tools are recommended. What the in-situ method measures is the change of sound pressure difference along the thickness direction of the liner, which reflects the local acoustic absorption and reflection performance. Therefore, the structure of the acoustic liner is preferred to be the locally resonant type.

Recently, Jing et al. [10] proposed a method to directly educe acoustic impedance in the flow duct (Straight forward method, SFM). According to the induct sound wave theory, regardless of the inlet and outlet acoustic boundary conditions, the sound pressure in the flow duct wall can be written as the sum of complex exponential functions. The specific expression is

$$p(x) = \sum_{n=1}^N A_n e^{-jk_{x,n}x} \quad (6)$$

where N is the number of cut-on modes, and A_n is the complex amplitude of sound pressure. The real part of $k_{x,n}$ is the forward propagating wave number. In the experimental flow duct device, the upstream and downstream sections close to the acoustic liner-installed section are all inner-hardwall ducts. The frequency of the incident sound wave generated by the loudspeakers is below the high modes cut-on frequency of the duct; therefore, only the plane wave propagates in the duct. In the liner-installed section, higher wave modes emerge in the flow direction and the directions perpendicular to the acoustic liner surface, because of the impedance of the liner. Therefore, the wave number of the modes in the duct are complex, indicating that the wave is attenuating. Impedance discontinuity at the leading and ending edges of acoustic liner will inevitably scatter multiple acoustic modes, and several acoustic modes will also be generated by the anechoic termination, although ideally it would not reflect any sound wave. All these factors make sound field in the flow duct complicated. The straightforward method is referred to as the concept of the Prony method from the electromagnetic discipline. It is applied to decompose the sound field into space modes, rather than the decomposition into complex time signals. After a complex wave number of a single wave is obtained, its normal wave number, $k_{y,n}$, can be calculated through the constraint relationship in different directions. The acoustic impedance can be directly obtained by substituting it into an eigen equation, as seen in Formula (7).

$$z = \frac{j(k - Mak_x)^2}{k \cdot k_y \cdot \tan(k_y b)} \quad (7)$$

The number of modes decomposed by the straight forward method is related to the number of microphones in measurement. When 16 microphones are used, up to eight modes can be decomposed. The straight forward method uses the mode with highest amplitude to calculate the acoustic impedance. Such a method does not require inserting the microphone into test samples; therefore, no physical damage to the structure will happen. The microphones measure sound pressure changes along the flow direction, which requires a minimal length of the test sample. Its tested results reflect the overall sound absorption performance of the acoustic liner and suggest no requirement limitation on the structural types of absorbent material; therefore, more forms of liner (Helmholtz resonator, foamed metal, etc.) could be tested with the straight forward method.

2.2. Acoustic Liner Impedance Eduction Experimental Device

The acoustic liner impedance eduction experiment mainly uses a flow tube to simulate the working environment of the acoustic liner in aeroengines. In the current study, the flow tube device used is shown in Figure 3 [15]. According to its functionality, the flow tube device can be divided into multiple modules: ① Acoustic measurement module, including a test sample (liner) installation box and a microphone array. The effective size of the test piece is 400 mm × 50 mm, and the walls on other sides of in this section are rigid walls. When the straight forward method is used, the upper wall of the section (opposite to liner) will be replaced with an array of 16 equally spaced microphones and a plate installing them. Two groups of three other microphones are arranged upstream and downstream in the acoustic measurement section. All microphones are flush-mounted to measure sound pressure. When the in-situ method is used, microphones are installed inside the liner sample. They are located at the same flow-wise direction and installed deep into different honeycomb cells. The first microphone head is flushed with the surface of a perforated plate, or the surface of middle layer perforation plate (when double degree of freedom liner is tested), and the second microphone is flush with the back plate, as shown in Figure 4; ② The flow field test modules are located upstream and downstream of the acoustic measurement section. Pressure sensors are used to determine the air flow velocity in the duct and measure the boundary layer thick-ness; ③ The sound source module, located upstream in the acoustic measurement module, uses loudspeakers with good broadband characteristics and a specially designed throat to maximize performance; and ④ The anechoic end modules are used to reduce the irrelevant noise transmitted from the upstream, and to reduce the acoustic reflection from the downstream duct exit. They are used to provide a non-reflective boundary, hence improving the quality of the acoustic field in the measurement section [15,16].

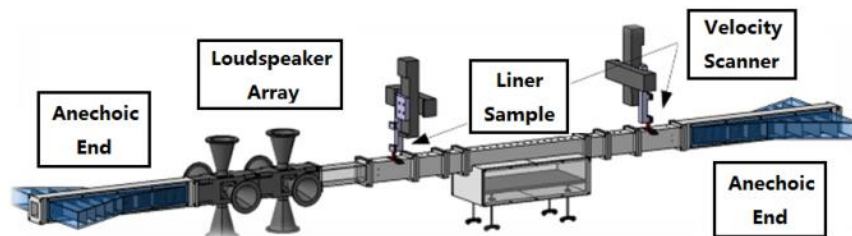


Figure 3. Schematic of impedance flow duct experimental platform.

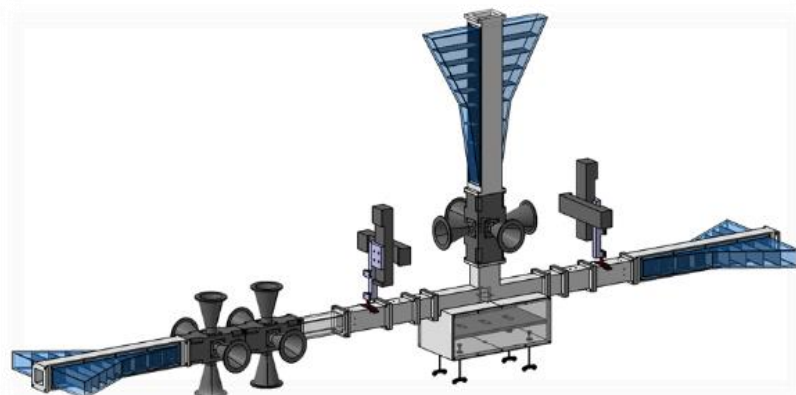


Figure 4. Schematic of in-situ method setup.

The duct cross section is a 50 mm × 50 mm square. The cut-off frequency in the duct at different flow velocities is

$$f_c = \frac{2}{c} \sqrt{\left(\frac{n_x}{l_x}\right)^2 + \left(\frac{n_y}{l_y}\right)^2} * \sqrt{1 - Ma^2} \quad (8)$$

where n_x and n_y are the orders in two directions perpendicular to the flow; and l_x and l_y are the lengths in two directions. The plane wave cut-off frequency is shown in Table 1.

Table 1. Cut-off frequencies at different Mach numbers.

Ma	0	0.085	0.18	0.26
f_c/HZ	3400	3387	3344	3283

To compare the actual performance of the two eduction technologies, a single degree of freedom (SDOF) acoustic liner (as shown in Figure 5) was tested for comparison. Its structural parameters are: $d_{im} = 1.2$ mm is the aperture of the perforated holes; $t = 1.2$ mm is the thickness of perforated plate; $\sigma = 7.62\%$ is the perforation ratio; $h = 18$ mm is the honeycomb height; and $s = 8.6$ mm is the width of opposite sides of the honeycomb core.

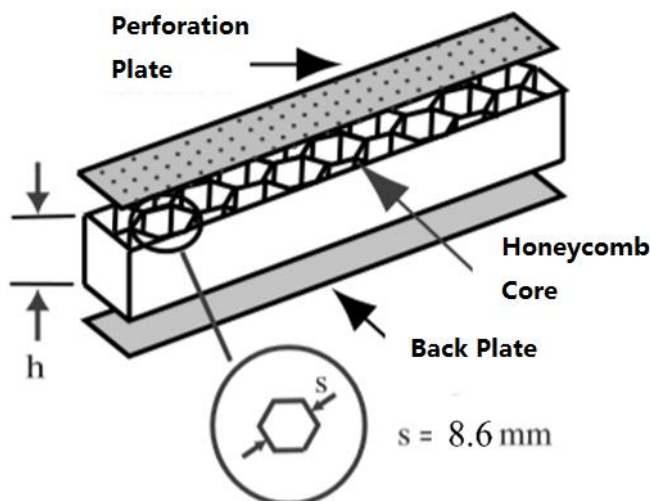


Figure 5. Schematic of tested SDOF liner.

Considering the cut-off frequency of the duct, the test frequency ranges from 100 to 4400 Hz, and the step interval is 100 Hz. The incident sound waves are excited by the loudspeaker array. The incident sound pressure level is above 130 dB. The microphone closest to the loudspeaker array is used as the reference.

2.3. Comparison of Two Methods for Acoustic Liner Impedance Eduction

As shown in Figure 6, the red line represents the result measured with the in-situ method (where the left-pointing triangle represents the acoustic resistance, and the down-pointing triangle represents the acoustic reactance). The black line represents the result measured with the straight forward method (where the right-pointing triangle represents the acoustic resistance, and the solid circle represents the acoustic reactance). The two sets of measured results generally agreed with each other in a wide frequency range, except for some obvious differences in the low frequency and high frequency ranges.

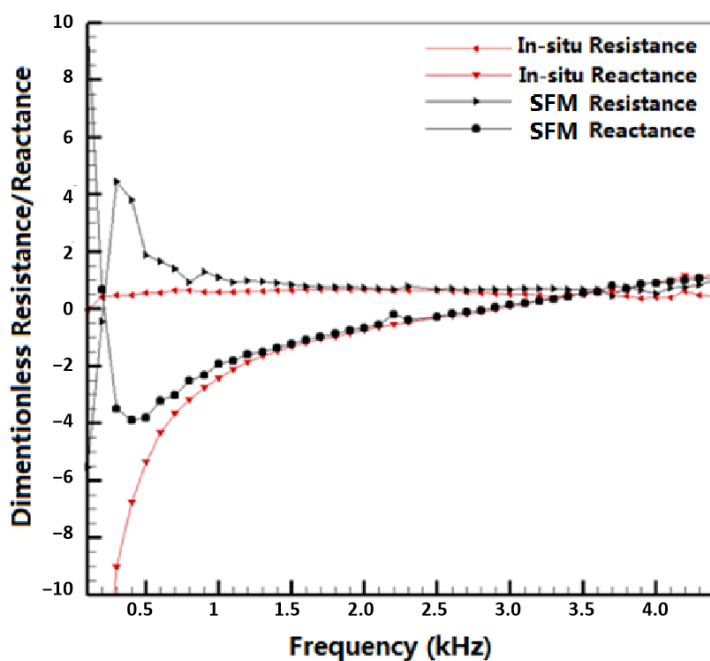


Figure 6. Comparison of measured results between in-situ method and straight forward method.

In the low frequency range of 100~400 Hz, the length of the liner sample is relatively short compared to the sound wavelength (the length of the liner is 400 mm). The liner's impedance has a limited effect on acoustic wave propagation, so an obvious fluctuation of acoustic resistance and reactance results could be observed, which leads to a lower accuracy of the straight forward method. The in-situ method in this frequency range, on the other hand, has little influence from the size of test sample, so its accuracy is considerably higher and acceptable. In the mid-frequency range of 3300~3800 Hz, high-order acoustic modes begin to appear in the flow tube, but the plane wave is still dominant. All microphones are in the center line of the duct wall, which is the stagnation point of high-order acoustic modes, so the test results are less affected and considerably usable. The two measurement methods have a good degree of coincidence in this range as well. In the high frequency range of 4000~4400 Hz, the amplitude of higher order acoustic modes in the duct is increasingly large. From the basic theoretic component of the straight forward method, namely the plane wave assumption, it no longer conforms to the actual situation. From the measurement results, the acoustic resistance measured by the straight forward method increases unexpectedly with the increase of frequency, which is also inconsistent with the common experiences of the acoustic resistance of the Helmholtz type acoustic liner. The in-situ method on the other hand, is not limited by the wave mode, but in actual experiments, the installation spacing of the two microphones also shows some sensitivity to the high-order modes in the flow tube. When the frequency continues to increase, the acoustic wave phase corresponding to the two microphones is different, so that the measured result begins to deviate from the theoretical value. From the measurement results, the acoustic resistance and reactance measured by the in-situ method also show some fluctuations, but it is smaller than those from the straight forward method. It can be shown that the measurement result from the in-situ method is more convincing in the high frequency band especially when higher acoustic modes exist in the flow tube device.

3. Acoustic Mode Synthesis and Detecting Technology for Nacelle Liner Test

3.1. Design Principle of Acoustic Spinning Mode Generator

During the development of acoustic liners, it is necessary to test samples for their acoustic manipulation effect, mainly measuring its modal suppression/scattering characteristics. Previous research has used full scale or reduced scale fans as acoustic sources.

However, because of the fixed acoustic mode character generated by the fan as the noise source, there are limitations to adjusting the mode number according to the extended experimental needs, which could lead to the insufficient verification of noise reduction performance of the acoustic liner sample. To generate more controllable acoustic modes and their combination, a feasible technical way is to use a special designed loudspeaker array that is uniformly distributed in the circumference direction on a casing and control it with phase regulation. Such an array would replace the rotating fan rotor as the acoustic source, which can also be used to measure the suppression or scattering effect of the acoustic liner on more mode setting. This technical way can also enable the development and validation of the nacelle liner before an actual engine/fan is built, hence improving the development efficiency.

Let the position coordinate of the observation point in an infinite circular duct be \mathbf{x} , and the sound pressure solution of multiple point sound sources in the duct be expressed as [17]

$$p(\mathbf{x}, \omega) = \sum_{l=1}^L \left\{ 1/2 \cdot Q_l \sum_{m=-\infty}^{\infty} \left\{ \exp[jm(\theta_0 - \theta_l)] \sum_{n=1}^{\infty} (G_{m,n,1}^c \cdot G_{m,n,2}^c) \right\} \right\} \quad (9)$$

$$G_{m,n,1}^c = \sum_{n=1}^{\infty} [J_m(k_{m,n}r_d) \cdot J(k_{m,n}r_0)] / \Gamma_{m,n} \quad (10)$$

$$G_{m,n,2}^c = \begin{cases} \exp[j(Mak_0 + k_{n,m})/(1 - Ma^2) \cdot (z_0 - z_l)] / k_{n,m} & \text{if } z_l > z_0 \\ \exp[j(Mak_0 - k_{n,m})/(1 - Ma^2) \cdot (z_0 - z_l)] / k_{n,m} & \text{if } z_l < z_0 \end{cases} \quad (11)$$

$$\Gamma_{m,n} = \pi(r_d^2 - \frac{m^2}{k_{mn}^2}) J_m^2(k_{m,n}r_d)$$

where L is the number of point sound sources, θ_0 is the circumferential angle of the observation point, θ_l is the circumferential angle of the point sound source number l , r_d is the radial position of the observation point, r_d is the radius of the duct, z_l is the axial coordinate of the point sound source, z_0 is the axial coordinate of the observer, and Q_l is the amplitude of the point sound source; $Ma = U/c$ is the Mach number in the duct; U is the flow velocity; $k_0 = w/c$ is the acoustic wave number; $J_m(\cdot)$ is the Bessel function of the m th order; $k_{n,m} = [k_0^2 - (1 - Ma^2)k_{mn}^2]^{1/2}$ is the characteristic value of the characteristic function.

It can be found that there is the expression that the amplitude of the circumferential mode and intensity of the point source are both linked with the term $\exp[jm(\theta - \theta_l)]$. By correlating it with point source amplitude Q_l , we can have

$$\left\{ \begin{array}{cccc} \exp(-i \cdot 1 \cdot \theta_1) & \exp(-i \cdot 1 \cdot \theta_2) & \dots & \exp(-j \cdot 1 \cdot \theta_{L-1}) & \exp(-j \cdot 1 \cdot \theta_L) \\ \exp(-i \cdot 2 \cdot \theta_1) & \exp(-i \cdot 2 \cdot \theta_2) & \dots & \exp(-j \cdot 2 \cdot \theta_{L-1}) & \exp(-j \cdot 2 \cdot \theta_L) \\ \vdots & \vdots & \vdots & \vdots & \vdots \\ \exp(-i \cdot (M-1) \cdot \theta_1) & \exp(-i \cdot (M-1) \cdot \theta_2) & \dots & \exp(-j \cdot (M-1) \cdot \theta_{L-1}) & \exp(-j \cdot (M-1) \cdot \theta_L) \\ \exp(-i \cdot M \cdot \theta_1) & \exp(-i \cdot M \cdot \theta_2) & \dots & \exp(-j \cdot M \cdot \theta_{L-1}) & \exp(-j \cdot M \cdot \theta_L) \end{array} \right\} \cdot \left\{ \begin{array}{c} Q_1 \\ Q_2 \\ \vdots \\ Q_{L-1} \\ Q_L \end{array} \right\} = \left\{ \begin{array}{c} A_1 \\ A_2 \\ \vdots \\ A_{M-1} \\ A_M \end{array} \right\} \quad (12)$$

Each line in Equation (12) corresponds to a circumferential modal order. Amplitude of each mode could be manipulated by tuning the amplitude and phase of point sound sources and their position θ in the duct.

The dimension of first matrix on the left of Equation (12) is $M \times L$. To make the equation solvable, $M \leq L$ is required. When the number of point sound sources L is determined, the maximum controllable number of circumferential orders would be M . In addition, considering $\sum_{l=1}^L \left\{ Q_l \sum_{m=-\infty}^{\infty} [\exp(-im\theta_l)] \right\}$ is a function whose period is L , namely

$$\sum_{l=1}^L \left\{ Q_l \sum_{m=-\infty}^{\infty} [\exp(-jm\theta_l)] \right\} = \sum_{l=1}^L \left\{ Q_l \sum_{m=-\infty}^{\infty} [\exp(-j(m+L)\theta_l)] \right\}, \quad (13)$$

when a target circumferential mode m is formed in the duct, modes with the $m \pm L$ order will also be formed (for cut-off modes, although it can be formed, it will not propagate to a long-distance position), so it is not expected to achieve a propagating mode beyond the range of $-L/2 + 1 \leq m \leq L/2 - 1$ by controlling a limited number of point sound sources [18].

3.2. Experimental Device of Acoustic Spinning Mode Generator

In total, 22 loudspeakers are uniformly distributed along the circumferential direction of a duct. According to the design principle, a specified circumferential acoustic mode can be formed when tuning the amplitude and phase of each loudspeaker. In the current study, a device with a tubular duct shape was built to validate the theory. The inner diameter is 0.26 m, and the outer diameter is 0.35 m. The maximum flow velocity in the duct is $Ma = 0.3$ and maximum frequency is 3000 Hz. The controllable circumferential mode ranges from 0 to 8. According to the duct geometry and flow velocity, higher radial mode will be cut-off, and only a certain amount of circumferential acoustic modes can propagate. As shown in Figure 7, an experimental device simulating engine exhaust duct is assembled from the numbers of sections. They are arranged in a flow-wise direction as the transition section, flow field test section, acoustic spinning mode generator, diversion section, acoustic mode detection section (upstream of acoustic liner), test sample section (to install liner or hardwall sample), acoustic mode detection section (downstream of acoustic liner), exhaust nozzle and central cone. The acoustic mode detection sections are designed as two types. The first type has a number of microphones fixed in a circle at different circumferential angles, and data is processed with the cross-correlation method [19]. The second type uses a rotating casing and scanning rake to study the scattering and reflection of the acoustic mode by the liner measure [20,21]. Acoustic mode detection sections are set both upstream and downstream, close to the test sample section.

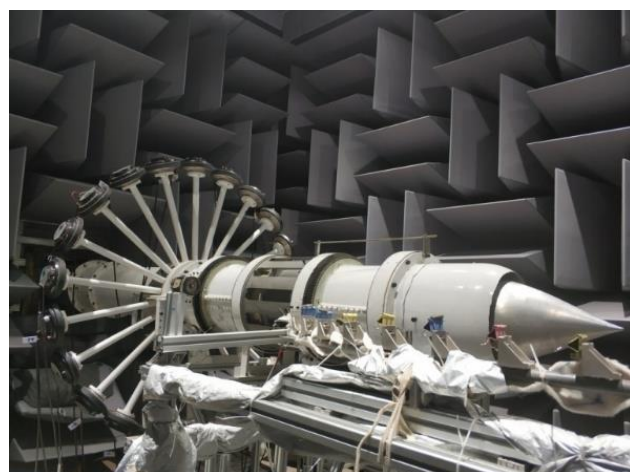


Figure 7. Experimental device of spinning mode generator and other sections assembly.

3.3. Verification of Acoustic Spinning Mode Generator

To test the capability to generate and control the single “pure” mode by the device, tests were carried out under a flow speed of $Ma = 0.3$. Acoustic excitation signals with $f_0 = 1250$ Hz and $f_0 = 2000$ Hz were given to generate the $(3, 0)$ mode and $(5, 0)$ mode, respectively. One can use the “Target Versus Aliasing (TVA)” value to judge if the device’s capability is good enough for further test usage. As shown in Figures 8 and 9, at 1250 Hz $(3, 0)$ mode case, the TVA value is higher than at 13 dB. At the 2000 Hz $(5, 0)$ mode case, the TVA value is higher than 21 dB. They both indicate good performance by the generation device.

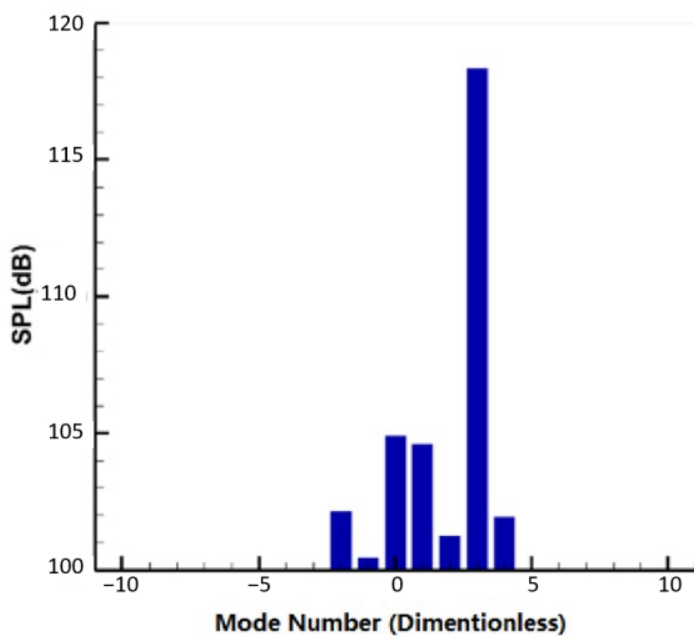


Figure 8. (3, 0) circumferential modes result at 1250 Hz.

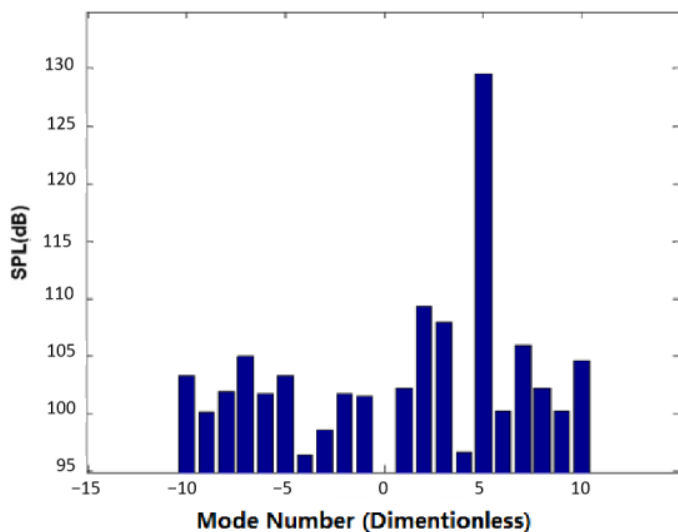


Figure 9. (5, 0) circumferential modes result at 2000 Hz.

4. Experimental Validation of Noise Reduction of Full-Size Nacelle Acoustic Liner

4.1. Experimental Setup

Another full-size nacelle acoustic liner experimental setup was built and is shown in Figure 10. The tonal fan noise source is simulated by another acoustic mode generator, which is composed of 32 loudspeakers uniformly distributed along the circumference direction and a controlling signal generating system. The inner surface of the acoustic mode generator is cylindrical with a diameter of 1.55 m. Another acoustic mode detecting ring device also consisting of 32 uniformly distributed microphones in the circumference direction is deployed between the acoustic mode generator and the nacelle inlet. According to the acoustic mode generation methodology described in Section 2.1 and the actual cut-off characteristics of tested inlet duct sample, the acoustic mode generation system can realize the generation and measurement of the 0~15th circumferential order acoustic modes under 2000 Hz.

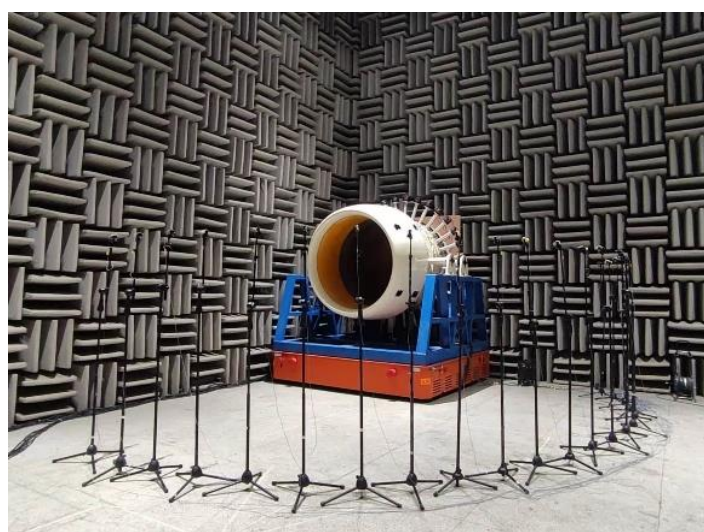


Figure 10. Full size nacelle acoustic liner experimental setup.

The far field directivity measurement consists of 21 microphones, evenly distributed in $0\text{--}120^\circ$ angle range (0° direction is the downstream of flow wise direction), and each microphone has a 6° interval. The directivity circular center is located at inlet lip, with a radius of 4 m. The microphone measuring plane is at the same height as the axis of the inlet setup, with all the microphones pointing towards the circular center of the inlet lip surface.

A total of three test pieces were used, including one solid wall/acoustic hardwall test piece, one metallic acoustic liner (or called “split acoustic liner”) designed and manufactured with traditional technology, and one composite seamless acoustic liner with an axial segmented design and wire mesh to provide additional acoustic resistance (also called a “seamless acoustic liner”). The inner diameters of the three test pieces are all 1550 mm, with the same total axial lengths of 650 mm. Both acoustic liner test pieces are designed for the noise suppression target of a certain type of aero-engine, that is, to match the target frequency and special acoustic mode radiating outward from that engine. For different operating conditions, the target frequencies mainly concerned include 1250 Hz and 2000 Hz. The circumferential acoustic modal excitation characteristics are determined according to the number of the rotor and stator of the engine fan. It is necessary to verify the noise reduction effect of both liners under experimental conditions. Table 2 shows the key experimental inputs and test conditions accordingly.

Table 2. The designed test conditions and experimental excitation.

Excitation Frequency	Acoustic Modes Order in Circumferential Direction	Acoustic Directivities Test
1250 Hz	9, 10, 12, 15	$0\text{--}120^\circ$
2000 Hz	9, 10, 12, 15	$0\text{--}120^\circ$

The “split acoustic liner” is shown in Figure 11. Its material and manufacturing process mainly reflects state-of-the-art 2000s’ technology. The perforation plate and rigid backplate are both made from a 2024-T62 aluminum sheet, whereas its acoustic perforations/apertures and riveting holes are all mechanically drilled. The honeycomb core is made from 5052 Aluminum. The plates and core are glued with epoxy-based cement with an acrylonitrile-butadiene rubber (NBR) modifier. An obvious riveting seam assembling different liner parts in circumference direction could be seen on inner surface of the test piece. The main structural parameters of the “split acoustic liner” test piece are shown in Table 3.

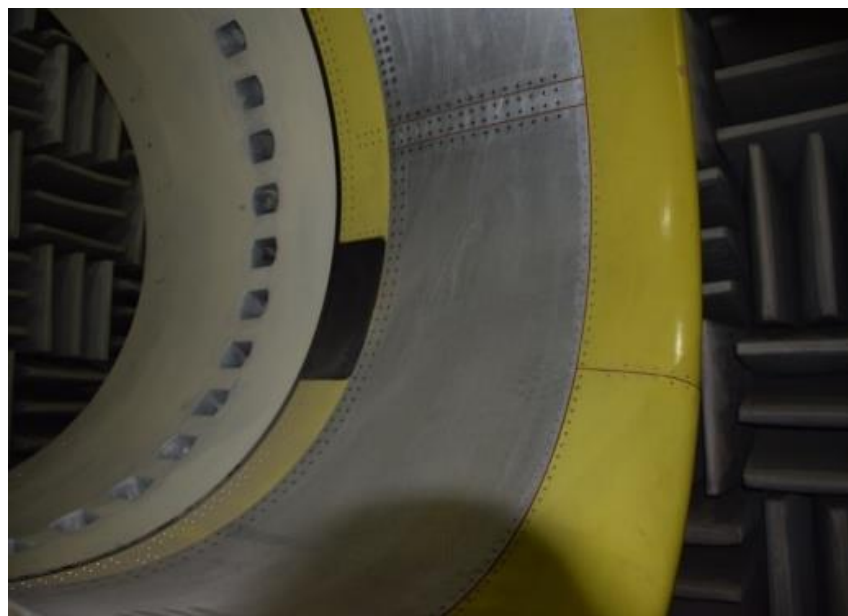


Figure 11. Test piece of “split acoustic liner”.

Table 3. Structure parameters of “split acoustic liner”.

Parameter	Value	Material
Panel thickness/mm	1	2024-T62
Hole size/mm	1	/
Perforation ratio/%	6.55	2024-T62
Honeycomb height/mm	30	5052 Aluminum

The seamless acoustic liner test piece is an axial segmented one that is seamless in the circumference direction, and uses the latest composite manufacturing process, as shown in Figure 12. The perforation plate and rigid backplate are both made from fiber glass (3162/SW-220-90A) prepreg. The honeycomb core is made from NOMEX®. The plates and core are mainly made by the resin transfer molding (RTM) process, and Automated fiber placement (AFP) is also applied in the area where additional strength is required. The acoustic perforations/apertures are all mechanically drilled after the curing process. Unlike the conventional ones, the inner surface of the “seamless acoustic liner” has no joining area that normally has different acoustic impedance and, hence, decreased noise reduction performance. An additional micro-diameter fine metal (stainless steel in current study) wire mesh is installed on the perforated plate to provide more acoustic resistance to improve broadband performance. Two segmented sections were designed and manufactured to have differences in hole diameter, perforation ratio and honeycomb core height configuration, in order to represent different impedance results. The main structural parameters of the “seamless acoustic liner” test piece are shown in Table 4. It can be observed that the perforation ratio is much higher than conventional ones, simply because the perforated plate is no longer the main contributor to acoustic resistance. The metal wire mesh will lead to much larger resistance, so the perforation ratio is no longer to be kept in the “old” optimal mode.



Figure 12. Test piece of “seamless acoustic liner” with zero splice.

Table 4. Main structure parameters of acoustic liner with zero splice.

Parameter	Value		Material
	Segment A	Segment B	
Panel thickness/mm	1.2	1.2	Fiber glass
Hole size/mm	1.3	3.3	/
Wire mesh count	635	635	Stainless steel
Perforation ratio/%	30	18	/
Honeycomb height/mm	18	40	NOMEX®

4.2. Noise Reduction Performance Test of Full Size Acoustic Liner Using Spinning Acoustic Mode Generator

As shown in Figure 13, under the set working condition (1250 Hz), the split acoustic liner has a certain amount of noise reduction between the 18–42° and 54–90° directional angle sectors, and the maximum noise reduction occurring at 72° is about 12.6 dB. However, the noise reduction performance at other angles is very limited, and even increases at some angles. Here, we define “peak to peak noise reduction” as the directional peak SPL from the acoustic liner minus the directional peak SPL under the hardwall test piece. By using this definition, the noise reduction of the split acoustic liner is about −10 dB, which means the peak noise increases by 10 dB. Furthermore, the directivity maximum has shifted from 60° (hardwall) to 0° (split acoustic liner).

The seamless acoustic liner has shown better noise reduction performance at almost all angles. In most angles, it shows more than 10 dB of noise reduction. Especially at 48–90°, the noise reduction exceeds over 20 dB. The peak-to-peak noise reduction is about 16.4 dB. Compared with the split acoustic liner, the noise reduction performance from the seamless liner has been greatly improved.

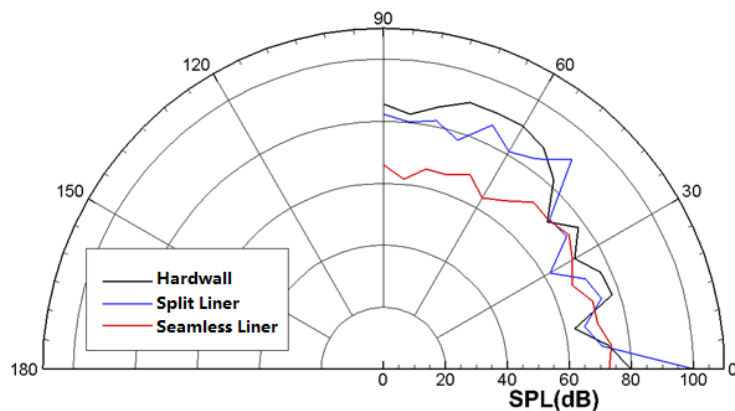


Figure 13. Acoustic directivity of (15, 0) circumferential mode at 1250 Hz.

As shown in Figure 14, under another working condition (2000 Hz), the maximum noise reduction of the split acoustic liner is about 35.4 dB at 54° , but the noise increases between $0\text{--}35^\circ$ and $72\text{--}90^\circ$, which indicates that the noise reduction performance at this frequency is achieved at the expense of the noise reduction performance at other angles. By the peak-to-peak noise reduction definition, the noise reduction of the segmented acoustic liners is close to -3.9 dB, which means that the peak noise increases. The seamless acoustic liner shows considerable better noise reduction performance at all angles; eat angles that range from 0° to 60° especially, more than 10 dB of noise reduction could be obtained, and the peak-to-peak noise reduction is about 9.1 dB. Compared with the split acoustic liner, the noise reduction performance is significantly improved by more than 13 dB.

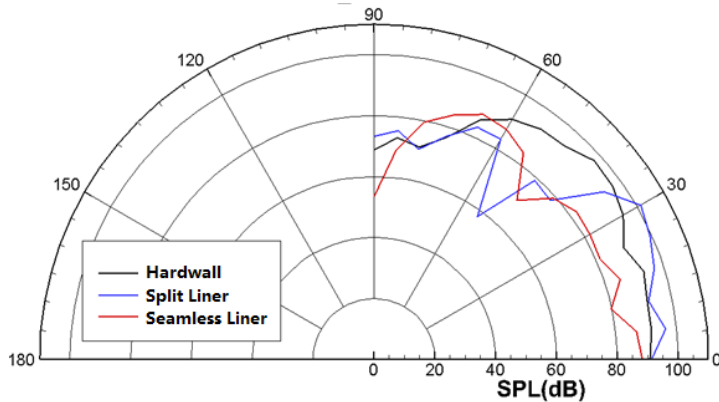


Figure 14. Acoustic directivity of (15, 0) circumferential mode at 2000 Hz.

In order to further study the main mechanism of noise reduction improvement from the seamless liner, the mode generator is used experimentally to send out numbers of separate and standalone acoustic modes in turn, and then modal noise reduction from every mode by two types of acoustic liner test pieces are compared. As shown in Table 5, the peak-to-peak noise reduction performance of a split acoustic liner under the 10th, 12th, and 15th circumferential modes at both 1250 Hz and 2000 Hz is negative, which indicates the failure of the noise reducing function under those working conditions. Under the 15th circumferential mode at 1250 Hz, as well as the 12th circumferential mode at 2000 Hz, noise reduction is -10 dB and -15.4 dB, respectively. This clearly indicates an insufficient design in split acoustic liner test pieces at both working conditions. It is also the main mechanism leading to its very limited overall noise reduction performance. The seamless liner, on the other hand, shows significant improvement. It could effectively suppress multiple modes under various frequencies, which is the main factor in achieving better overall noise reduction performance versus split acoustic liners in various working conditions.

Table 5. Analysis of noise reduction under different acoustic modes excitation.

Excitation	Hardwall/dB	Split Acoustic Liner		Seamless Liner		
		SPL/dB	Noise Reduction/dB	SPL/dB	Noise Reduction/dB	Improvement/dB
1250 Hz, 9th Mode	98.5	98.2	0.3	83.6	14.9	14.6
1250 Hz, 10th Mode	96.9	99.2	-2.3	91.3	5.6	7.9
1250 Hz, 12th Mode	83.9	90.7	-6.8	74.9	9	15.8
1250 Hz, 15th Mode	90.4	100.4	-10	74.1	16.3	26.3
2000 Hz, 9th Mode	93.8	91.6	2.2	86.4	7.4	5.2
2000 Hz, 10th Mode	95.8	105.2	-9.4	84.8	11	20.4
2000 Hz, 12th Mode	91.9	107.3	-15.4	84.6	7.3	22.7
2000 Hz, 15th Mode	97.4	101.4	-4	88.3	9.1	13.1

5. Conclusions

Two kinds of experimental technology evaluating aircraft nacelle acoustic performance were developed: acoustic impedance eduction and acoustic mode synthesis technology. Verification tests were also carried out using both technologies. The main conclusions are as follows:

(1) The acoustic impedance eduction technology based on the in-situ method and the straight forward method both show good accuracy in the medium frequency range. Differences in dimensionless acoustic impedance and dimensionless acoustic impedance are both less than 0.2. The in-situ method has higher accuracy in low frequency range. In the high frequency range, the accuracy of both methods decreases, but the reliability of the in-situ method is higher.

(2) The acoustic spinning mode generator based on the phase array control method can produce single “pure” modes and their combination through fine phase and amplitude control, which can be used for verification experiments on a nacelle acoustic liner.

(3) The spinning mode generator was used to carry out an experimental study on two types of full-size inlet liner. Compared with the split liner manufactured through the previous process, the new seamless acoustic liner realized with the latest composite technology has significantly improved the noise reduction effect at multiple acoustic modes and frequencies, introducing further noise reduction capability.

Author Contributions: Conceptualization, Q.Y. and D.X.; methodology, D.X. and J.Y.; validation, X.G., D.X. and J.Y.; formal analysis, Q.Y.; investigation, D.X.; resources, W.H.; data curation, X.G.; writing—original draft preparation, Q.Y. and D.X.; writing—review and editing, Q.Y. and Q.M.; funding acquisition, Q.Y. All authors have read and agreed to the published version of the manuscript.

Funding: This research was funded by the National Science and Technology Major Project (2017-//0005-0016).

Institutional Review Board Statement: Not applicable.

Informed Consent Statement: Not applicable.

Data Availability Statement: Not applicable.

Conflicts of Interest: The authors declare no conflict of interest.

References

- Nark, D.M.; Jones, M.G. An Investigation of Bifurcation Acoustic Treatment Effects on Aft-Fan Engine Nacelle Noise. In Proceedings of the 25th AIAA/CEAS Aeroacoustics Conference, Delft, The Netherlands, 20–23 May 2019.
- Envia, E. Fan noise reduction—an overview. In Proceedings of the 39th Aerospace Sciences Meeting and Exhibit, Reno, NV, USA, 8–11 January 2001.
- Wang, X.Y.; Sun, X.F. Transfer element method with application to acoustic design of aero-engine nacelle. *Chin. J. Aeronaut.* **2015**, *28*, 327–345. [[CrossRef](#)]
- Dean, P. An in situ method of wall acoustic impedance measurement in flow ducts. *J. Sound Vib.* **1974**, *34*, 97–130. [[CrossRef](#)]
- Zandbergen, T. On the practical use of a three-microphone technique for in-situ acoustic impedance measurements on double layer flow duct liners. In Proceedings of the 7th Aeroacoustics Conference, Palo Alto, CA, USA, 5–7 October 1981.
- Watson, W.R.; Jones, M.G.; Parrott, T.L. Validation of an impedance education method in flow. *AIAA J.* **1999**, *37*, 818–824. [[CrossRef](#)]

7. Jones, M.G.; Watson, W.R.; Tracy, M.B.; Parrott, T.L. Comparison of two waveguide methods for educating liner impedance in grazing flow. *AIAA J.* **2004**, *42*, 232–240. [[CrossRef](#)]
8. Watson, W.R.; Tanner, S.E.; Parrott, T.L. Optimization method for educating variable-impedance liner properties. *AIAA J.* **1998**, *36*, 18–23. [[CrossRef](#)]
9. Jones, M.G.; Watson, W.R. Effects of liner length and attenuation on NASA Langley impedance education. In Proceedings of the 22nd AIAA/CEAS Aeroacoustics Conference, Lyon, France, 30 May–1 June 2016.
10. Jing, X.D.; Peng, S.; Sun, X.F. A straightforward method for wall impedance education in a flow duct. *J. Acoust. Soc. Am.* **2008**, *124*, 227–234. [[CrossRef](#)] [[PubMed](#)]
11. Qiu, X.; Xin, B.; Jing, X. Straightforward impedance education method for non-grazing incidence wave with multiple modes. *J. Sound Vib.* **2018**, *432*, 1–16. [[CrossRef](#)]
12. Chen, L.; Du, L.; Wang, X.; Jing, X.; Sun, X. A three-dimensional straightforward method for liner impedance education in uniform grazing flow. *J. Sound Vib.* **2019**, *468*, 115119. [[CrossRef](#)]
13. Loew, R.; Lauer, J.; Mcallister, J.; Sutliff, D.L. The advanced noise control fan. In Proceedings of the 25th AIAA Aerodynamic Measurement Technology and Ground Testing Conference, San Francisco, CA, USA, 5–8 June 2006.
14. Tapken, U.; Raitor, T.; Enghardt, L. Tonal noise radiation from an UHBR fan—Optimized in-duct radial mode analysis. In Proceedings of the 15th AIAA/CEAS Aeroacoustics Conference (30th AIAA Aeroacoustics Conference), Miami, FL, USA, 11–13 May 2009.
15. Yang, J.F.; Xue, D.W.; Li, Z.H.; Huang, T.; Xu, J. Single and double degree-of-freedom acoustic liners under grazing flow: Experiment. *Acta Aeronaut. Astronaut. Sin.* **2020**, *41*, 223860.
16. Xin, B.; Yang, J.; Jing, X.; Sun, X. Experimental and numerical investigation of anechoic termination for a duct with mean flow. *Appl. Acoust.* **2018**, *139*, 213–221. [[CrossRef](#)]
17. Davies, P. Practical flow duct acoustics. *J. Sound Vib.* **1988**, *124*, 91–115. [[CrossRef](#)]
18. Yan, Q.; Xue, D.W.; Huang, W.C.; Gao, X. Design of acoustic spinning mode synthesizer and its application in aeroengine nacelle liner validation experiment. In Proceedings of the 15th Russia-Chinese Conference, TsAGI, Zhukovsky, 17–18 July 2017.
19. Sijtsma, P.; Zillmann, J. In-duct and far-field mode detection techniques. In Proceedings of the 13th AIAA/CEAS Aeroacoustics Conference (28th AIAA Aeroacoustics Conference), Rome, Italy, 21–23 May 2007.
20. Tapken, U.; Enghardt, L. Optimization of sensor arrays for radial mode analysis in flow ducts. In Proceedings of the 12th AIAA/CEAS Aeroacoustics Conference (27th AIAA Aeroacoustics Conference), Cambridge, MA, USA, 8–10 May 2006.
21. Sutliff, D.L. Rotating rake turbofan duct mode measurement system. *J. Acoust. Soc. Am.* **2005**, *118*, 1864. [[CrossRef](#)]

Disclaimer/Publisher’s Note: The statements, opinions and data contained in all publications are solely those of the individual author(s) and contributor(s) and not of MDPI and/or the editor(s). MDPI and/or the editor(s) disclaim responsibility for any injury to people or property resulting from any ideas, methods, instructions or products referred to in the content.